

## Time Response of a Resonant Tunneling Diode Based Photo-Detector (RTD-PD)

Mohammad Ahmadzadeh<sup>1</sup>, Abbas Ghadimi<sup>\*,2</sup>, Seyed Ali Sedigh Ziabari<sup>1</sup>

<sup>1</sup> Department of Electrical Engineering, Rasht Branch, Islamic Azad University, Rasht, Iran

<sup>2</sup> Department of Electrical Engineering, Lahijan Branch, Islamic Azad University, Lahijan, Iran

(Received 20 Dec. 2020; Revised 28 Jan. 2021; Accepted 24 Feb. 2021; Published 15 Mar. 2021)

**Abstract:** In this article, a resonant tunneling diode with AlAs/GaAs double barrier structure using the non-equilibrium green's function is simulated. A lattice matched InGaAs absorption layer is added to the device for light detecting at the wavelength  $\lambda=600$  nm. The electric field through the device and energy band diagram profile were presented. The photo current of the device and source photocurrent curves versus light intensity are compared. At room temperature, the quantum efficiency of 0.95 was obtained for the device. Transient time response of the device was obtained and its dependencies on structural parameters (absorption layer thickness, collector and emitter thickness and doping of the contacts), light intensity, angle of emitted light and voltage bias were simulated and their influences on operation of the device were analyzed. Bandwidth of the device was obtained. The simulation results show that when voltage bias increases, fall time decreases and the response of the device is faster. With changing of absorption layer and contacts thicknesses, time response of RTD-PD changes. The variations of doping in contact layers effect on bandwidth. The result show that variations of light intensity and angle of emitted light change transient time response.

**Keywords:** Quantum Well, Absorption Layer, Time Response, Non-Equilibrium Green's Function (NEGF),

### 1. INTRODUCTION

Semiconductor photo detectors are the most suitable choice for different applications such as wireless communications [1], high-speed optical communications such as radio-over-fiber networks [2,3], Infrared [4] and bio-imaging for identifying cancers [5] due to their low cost, small size, strength, low power consumption, wide spectrum range, good sensitivity and fast response. Quantum devices such as RTDs work with ballistic constraints based on quantum

\* Corresponding author. Email: [ghadimi@liau.ac.ir](mailto:ghadimi@liau.ac.ir)

resonant tunneling theory. RTDs are nonlinear bits that cover a wide range of applications, one of them is photo detectors at telecommunications wavelengths [6]. Since the resonant tunneling phenomenon was discovered in heterojunctions consisting of group III and V semiconductors, double barrier resonant tunneling diode photo detectors (RTD-PD) have been used in many applications such as optical communications [7] due to the high RTD response speed [8]. The most important features of RTD-PD is its unique characteristic such as differential negative resistance, low working voltage, high quantum efficiency, low switch energy, lower noise factor, low cost and a simple structure [6].

Double barrier quantum well RTD based photo-detectors are interesting alternatives for optical detection when compared with traditional photo-detectors due to their photo detection mechanism and built in electrical gain arising from RTD's current-voltage (I-V) characteristic showing a region of negative differential resistance (NDR) [9]. In [10], a method for study on RTD that was applicable in high frequency, was presented. In [11], an InGaAs/AlAs resonant tunneling diode were studied using five different structures. In [12], output power of a RTD was analyzed theoretically. In [13], electrical properties of a three barriers (two well) resonant tunneling diode were modeled. In [14], the optoelectronic oscillators using a nonlinear dynamic solution were studied. In [15], Andreas Pfenning et al studied the sensitivity of a dual-barrier RTD-based photo detector with a GaInNAs absorption layer for light sensing at telecommunication wavelength, but they did not mention wavelength dependence of the detector performance. In [16], a RTD-based photo detector with nonconstant responsivity was introduced. In [17], a model was investigated based on two AlGaAs barriers and an InGaAs absorption layer. In [18], a resonant tunneling diode-based photo detector with dual absorption layer  $\text{In}_{0.53}\text{Ga}_{0.47}\text{As}$  was fabricated by the molecular beam epitaxy method at wavelength of 600 nm, but structural parameters dependency was not mentioned. In [19], a cavity enhanced RTD-PD for telecommunications applications was introduced. Optical and electrical Properties were explored at room temperature. In [20], Y dong and colleagues designed a resonant tunneling diode with a multiplication area for light detection. By adding a region, the sensitivity of the detector was set. In [21], a light detection at the wavelength of 1300 nm by adding a GaInAs layer to a GaAs based tunneling diode was achieved. In [22], Lee et al Showed that the wavelength of a quantum dot based detector can be extended to 1310 nm. In [23], the direct intensity modulation characteristics of a high speed RTD-PD with an oscillation frequency of 79 GHz was reported. In [24], Junzhe Geng et al presented a multi scale quantum transport model and used non-equilibrium green's function formalism to compute the dynamic(states) and kinetics (filling of states) of the device. In [25], latest academic quantum transport models were based on the non-equilibrium Green's function (NEGF) method that cover all coherent and incoherent quantum effects consistently. Carrier recombination and

generation in optoelectronic nano devices represent an immense numerical challenge when solved within NEGF. In [26], the implications of non-locality and localization for the implementation and performance of quantum optoelectronic device simulators based on the non-equilibrium Green's function formalism were considered. In [27], a photodiode with InGaAs absorption layer was presented operating in visible and near infrared wavelengths. In [28], critical thickness was determined for InGaAs/GaAs heterostructures. In [29], optical and electrical properties of the graphene was investigated. In [30] a quantum modeling of light absorption in graphene based device was presented.

## 2. Methodology

The equilibrium green's function is used to model the device, which incorporates a comprehensive physical structure that shows the behavior of the particles in the device. The non-equilibrium green's function is typically used as a matrix form in a computational cycle that contains information about the device's response to various excitation sources such as applied voltage. The different scattering sources such as phonons, electrons, impurities and boundary mismatches can be assumed to be an internal excitation source, and the final current can be the sum of the currents resulting from the effect of all sources. Silvaco presents a self-consistent solution between the Poisson and NEGF equations utilizing an effective mass Hamiltonian. The use of a multiple band effective mass band structure assumes they are parabolic and isotropic in the perpendicular plan which allows for the integration of carrier and current densities across  $\mathbf{k}$ -space analytically. A mode space approach is utilized where a NEGF formalism is applied in the transport direction and then coupled with Schrodinger's equation in the transverse plane. A planar approach, more suited to RTDs can also be used. This method assumes that the transverse plane is infinite. This model assumes ballistic transport therefore the calculated current is idealized. The equilibrium regions are further assigned a broadening parameter which is a small imaginary number added to the onsite potential of the Hamiltonian and is required to fill emitter quasi-bound states. Normally, these states are filled with electrons scattered by inelastic phonons. For this method, the device is broken into multiple regions: collector, emitter, non-equilibrium active region and spacer. The contacts and spacer are both considered to be in strong equilibrium, but the occupation factor varies based on the quasi-Fermi level on their respective sides. The active region is considered non-equilibrium. The model assumes that the emitter and collector regions are in quasi-equilibrium. The resistance of this regions is much smaller than of the central double barrier structure. The Green's functions are calculated for the active region as well as the spacer. However, the charge for the contacts is calculated with semi-classical methods.

In this research, a RTD based quantum well double barrier structure device is simulated by a numerical software. We use NEGF to model of the device. We

add an InGaAs absorption layer the device between collector and the barrier structure for transforming the structure into RTD-PD. The light at wavelength of 600 nm is illuminated on the device and diagrams related to device output specifications are obtained. Time response of the device is analyzed. For obtaining a reliable device we investigated the effectiveness of changing structural parameters like absorption layer thickness, collector-emitter thickness on time response of the device. We also study the effectiveness of variations of doping, light intensity, voltage bias, the angle of emitted light on transient time response of the RTD-PD. We obtained bandwidth of the device.

### 3. Results and Discussion

#### 3.1 Discussion

The 1D effective mass Hamiltonian is discretized in real space via a finite difference method [31]. The Schrodinger wave equation plays an important role, and the probability of tunneling an electron into a quantum well is calculated by solving the Green's equation and the Schrodinger wave equation. Discrete energy levels exist in the quantum structure that generate energy for the electrons to tunnel, called resonance levels. When the voltage is applied to the device, the electron is excited and its energy reaches to one of the resonant levels. This electron can tunnel through the barriers. The Hamiltonian is defined as:

$$H = -\frac{\hbar^2}{2m^*} \frac{d}{dx} \left( \frac{d}{dx} \right) + V_k + \frac{\hbar^2 k^2}{2m_{c2}^*} \quad (1)$$

Where  $m_{c2}^*$  is the effective mass of the emitter contact .

$$V_k(x) = V(x) + \frac{\hbar^2 k^2}{2m_{c2}^*} \left( \frac{m_{c2}^*}{m^*} - 1 \right) \quad (2)$$

The discretization of the Hamiltonian leads to a scalar matrix, without using an orbital based approach, then each element becomes a sub-matrix and disruptive ensues. For the interaction between the spacer and the non-equilibrium device region equation (3) is defined:

$$I = G_{DR} \left( E - H_{DD} - \sum_{cR} - \sum_{ER} \right) \quad (3)$$

Where  $\Sigma CR$  and  $\Sigma ER$  define the self-energies for the device interactions between the collector and emitter respectively.  $H_{DD}$  and  $G_{DR}$  are Hamiltonian of the device and the green's function of the device region respectively. It is here where the in-scattering self-energies, which define the broadening parameter. The broadening term ( $\eta$ ), is used to determine the density of states in the quasi-bound state:

$$D_{em}(E) = \frac{\eta(E)}{2\pi \left[ (E - \varepsilon)^2 + \eta(E)^2 \right]} \quad (4)$$

The electron density in the active region is determined with:

$$n_{ar} = 2 \int \frac{G(E)}{2\pi} dE \quad (5)$$

The energy levels are determined with:

$$E_n = \frac{\hbar^2 n^2}{8m^* w^2} \quad (6)$$

Where  $w$ ,  $n$ ,  $E_n$ ,  $\hbar$  and  $m^*$  are well width, number of resonant levels, resonant level energy, reduced Planck's constant and effective mass respectively. Non-equilibrium Green's function normalization is used to tunnel electrons into a quantum structure with ballistic conditions. The tunneling current density is shown below:

$$J = \frac{q}{2\pi\hbar} \int N(E) T(E) dE \quad (7)$$

Where  $\hbar$ ,  $T_{(E)}$  and  $q$  are reduced Planck's constant, the probability that the electron will radiate from the emitter and the electric charge respectively.  $N_{(E)}$  is shown as follows:

$$N_E = \frac{KTm^*}{\pi\hbar^2} \ln \left[ 1 + \exp \left( \frac{E_f - E}{KT} \right) \right] \quad (8)$$

Where  $E_f$ ,  $T$  and  $K$  are Fermi level of emitter, temperature in terms of Kelvin and Boltzmann constant. Basically, this model determines the carrier density and the Poisson's equation is solved, and then an energy grid is defined using the quantum

transmission boundary method and very narrow resonances occur. The solution of the non-equilibrium green's function is calculated with the details of the quantum charge density and this process is repeated until the convergence takes place. For the device all equations related to this type of detector such as carrier rate equations, carrier continuity equations, equations related to non-equilibrium green's functions and Poisson's equation are solved. The current of a single source of light is obtained from the following equation [31]:

$$I_s = q \frac{B_n \lambda}{\hbar c} w_t \quad (9)$$

Where  $B_n$ ,  $n$ ,  $\lambda$  and  $\hbar$  are the intensity, the number of light beams, wavelength and reduced Planck's constant respectively.  $C$  is the speed of light and  $w_t$  is the width of the beam that contains the effects of clipping. This is considered as a criterion for measuring the rate of radiation photons on the device. The available photocurrent divided by the source photocurrent is a measure of the external quantum efficiency of the detector [1]:

$$\eta_{ext} = \frac{I_{ph}}{I_s} \quad (10)$$

$I_{ph}$ , is photocurrent, wavelength, velocity of light and emitted optical signal. External responsivity also depends on wavelength and quantum efficiency, as follows [1]:

$$R \lambda = \frac{\lambda}{1.24} \eta_{ph} \quad (11)$$

Photo detector response time is the root mean square sum of the charge collection time and time constant arising from series load resistances and the junction and stray capacitances. Charge collection time is voltage dependent. The fast component is the transit time of the charge carriers (electrons and holes) through the depletion region, producing carriers that are collected by diffusion. The transient time of these carriers will be relatively slow. The detector active area thickness is related to the amount of time required for the electrons generated to flow out of the detector active area. This time is referred to as the electron **transient time**. The thicker active area, longer the transient time will be. Minimum limit on this active area exists to provide for efficient fiber-to-detector coupling. Trade-offs between fast transient times and low capacitance are necessary for high-speed response. However, any change in photodetector parameters to optimize the transient time and capacitance can also affect responsivity and coupling efficiency. A fast transient time requires a thin detector active area, while low capacitance and high responsivity require a thick active

region. The capacitance of the photodetector must be kept small to prevent the RC time constant from limiting the response time. The photodiode capacitance consists mainly of the junction capacitance and any capacitance relating to packaging the transient time of the photo carriers in the depletion region. The transient time depends on the carrier drift velocity( $v_d$ ) and the depletion layer width  $w$ , and is given by:

$$t_d = \frac{w}{v_d} \quad (12)$$

Response time is the time required for the detector to respond to an optical input. The response time is related to the bandwidth of the detector and is given by:

$$BW = \frac{0.35}{t_r} \quad (13)$$

Where  $t_r$  is the rise time of the device and it is the time that takes for the detector to rise to a value equal to 63.2% of its final steady-state quantity.

### 3.2 Simulation and Results

3.2a **Structure:** First, a quantum well double barrier resonant tunneling diode device is simulated. A schematic of the RTD layer sequences are shown in Fig.1. Double barrier resonant tunneling structure consist of two 2 nm wide AlAs barriers and a 2 nm wide GaAs quantum well. Two contacts are deposited on the top to form electrical contacts in top and bottom of double barrier structure. The thickness of the contacts is 30nm. The concentration of the contacts is  $10^{18}$ . Double barrier structure is undoped.

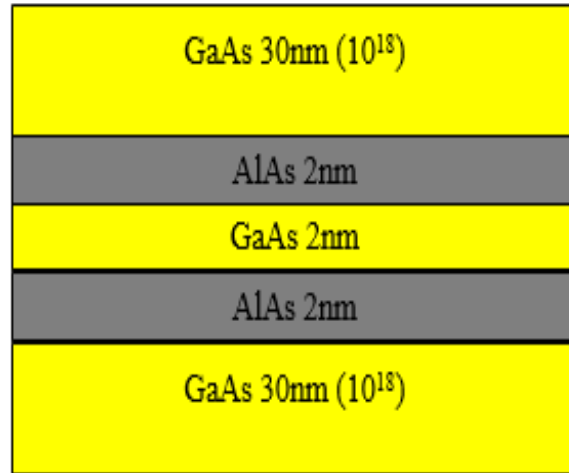


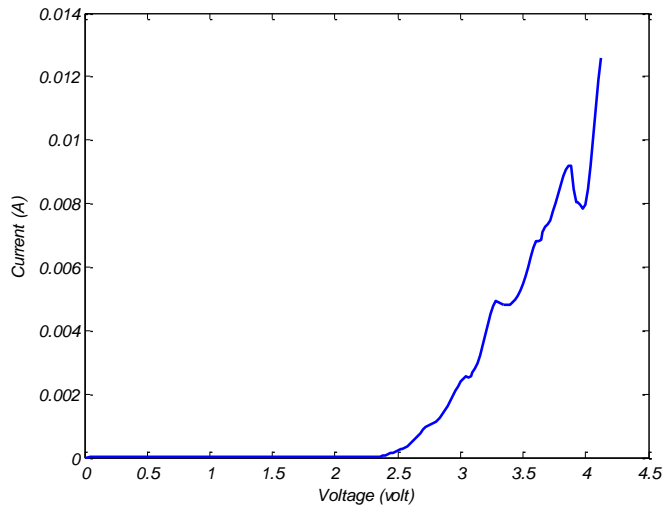
**Figure. 1.** schematic of the RTD layer sequences

The wave nature of electrons leads to quantum phenomena such as tunneling because wavelength of electron is comparable with dimension of double barrier quantum well structure. Table.1 shows details of structural parameters of RTD.

**Table 1**  
**Physical parameters of RTD**

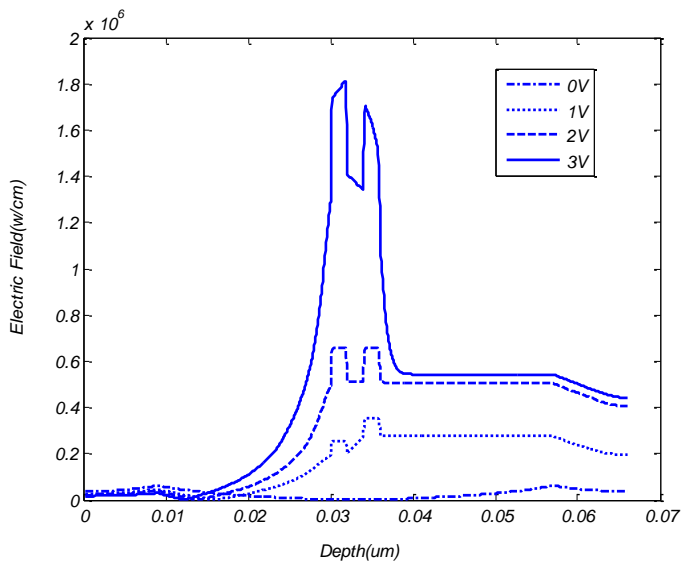
Region	Material	Size	Dopant(type )
barriers	AlAs	2 nm	undoped
well	GaAs	2 nm	undoped
Top contact	GaAs	30 nm	10 <sup>18</sup> (n)
Bottom contact	GaAs	30 nm	10 <sup>18</sup> (n)

Different voltages were applied to the device and the current–voltage (I–V) characteristics of the device at room temperature has been shown in Fig.2.



**Figure. 2.** Current-Voltage characteristic of the RTD

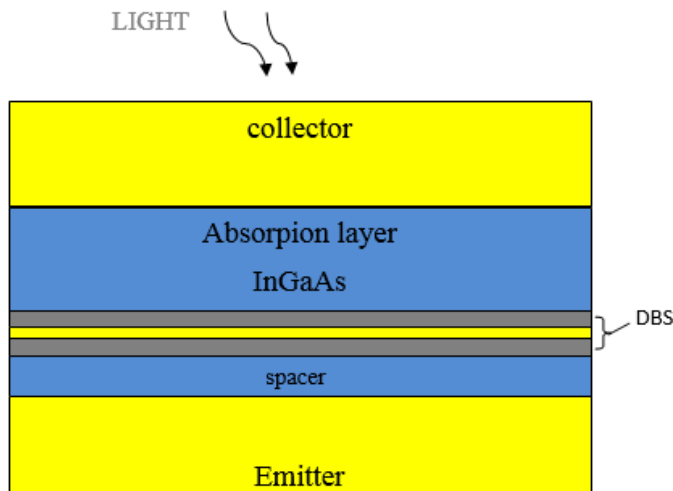
The current-voltage characteristic of the device shows a negative differential resistance (NDR) region. As seen, in this region, when the bias voltage increases, the current of the device decreases. This is due to the wave nature of the electron that we mentioned it. The electric field through the device in different voltages has been shown in figure 3.



**Figure. 3.** Electric field through the device at bias voltages from 0 V to +3 volt.

The voltage was changed from 0 V to +3 V. Figure.3 shows that the electric field in barriers is more than the other regions in 2 and 3 volts. The accumulated positive charge changes the electrostatic field and an additional voltage drop across the resonant tunneling structure. An overlap is created by electric field in energy levels between the emitter and one of the quasi-bound states within the QW, resulting in a tunneling current via the state.

To transform the structure into an RTD based photo detector, we add a 600 nm thick InGaAs absorption layer between collector and barrier structure for light absorption. There is an InGaAs spacer layer between the double barrier structure and emitter to avoid impure scattering of the emitter towards the barriers. The spacer layer thickness is 12 nm. The absorption layer and spacer layer are undoped. The physical structure of the resonant tunnel diode-based photo detector is shown in Fig. 4. The length of the cavity is 400 nm. We use a light source illuminated to the device. Light at wavelength of 600 nm with a radiation angle of 90 degrees radiates to the collector from a distance of 100 nanometers above the device. The light is absorbed by absorption layer. Electron-hole pairs are excited by incident photons emitted from light source to absorption layer. When an external electric field is applied to the device, photo generated holes' drift into the emitter side and accumulate at the interface between double barrier structure and absorption layer. The accumulated positive charge changes the electrostatic field and an additional voltage drop across the resonant tunneling structure can modulate resonant tunneling current of electrons. For inverse bias, there is no hole accumulation and the current vanish [17].



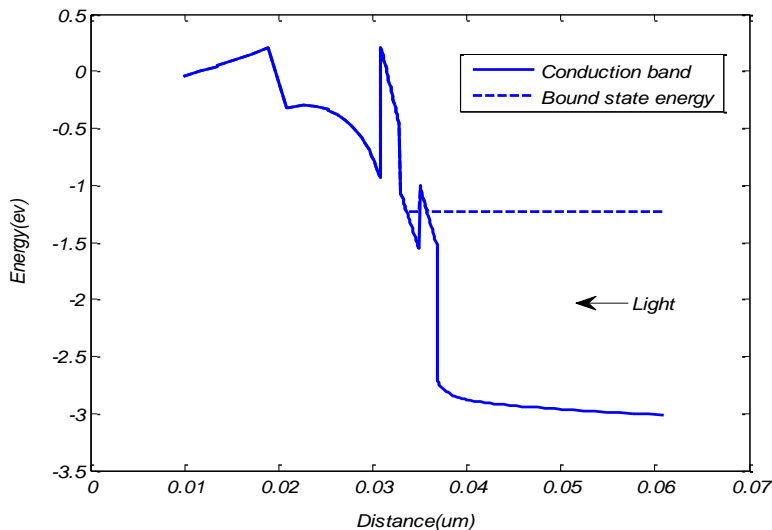
**Figure .4.** Resonance tunneling diode photodetector structure

Table. 2 provides detailed information on device design.

**Table 2**  
**Parameters of designing of the RTD-PD**

Region	Material	Size	Dopant(type )
barriers	AlAs	2 nm	undoped
well	GaAs	2 nm	undoped
absorption	InGaAs	600 nm	undoped
spacer	InGaAs	12 nm	undoped
collector	GaAs	30 nm	$10^{18}(n)$
emitter	GaAs	30 nm	$10^{18}(n)$

The conduction band profile of the RTD with absorption layer is shown in Fig.5. When some voltages are applied to the device then electron is excited and their energy reaches to the energy that equals to one of the resonant state. This electron can easily tunnel through the barriers [32]. Also, current-voltage characteristic of RTD with absorption layer has been shown in Fig.6.



**Figure .5.** The Conduction band profile of the RTD at bias of 4V and bound state energy level

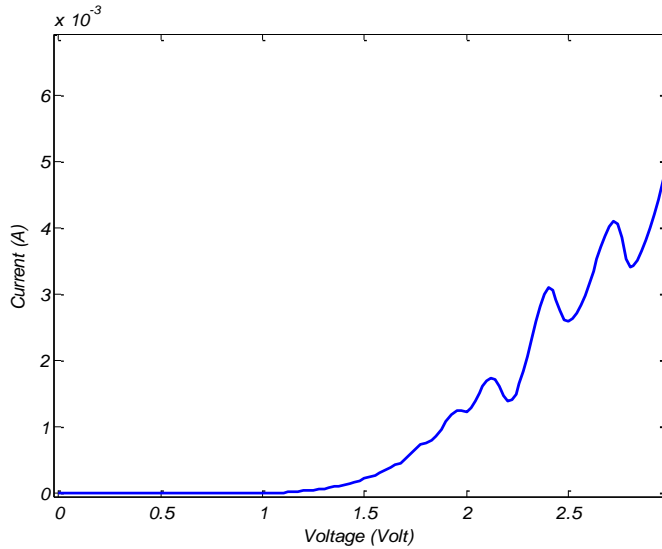


**Figure. 6.** Current-Voltage characteristic of the RTD with absorption layer

Source photocurrent and available photocurrent versus light intensity have been shown in Fig.7. The quantum efficiency of the device is 95%.

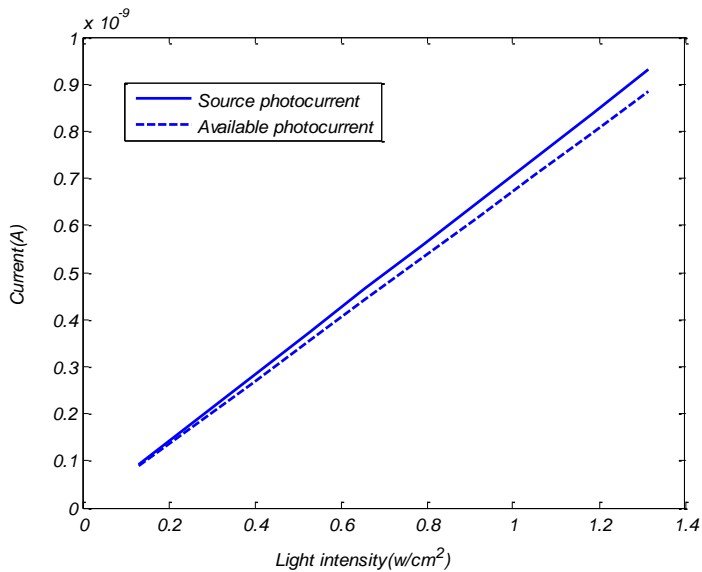


**Figure. 7.** Source photo current (solid) and available photo current (dash) versus light intensity

**3.2b Results:** For obtaining of time response of the device, the light intensity illuminated from the light source was changed linearly by defining some parameters in the software [31]. The period of this linear triangular signal is also defined. The maximum intensity in the simulation is 5 watts per square meter, the pulse width is 2 ns, and the response is calculated. Rise time for the pulse is 10 Pico second. The wavelength of the light is 600nm. First, the collector terminal current curve versus time is presented in figure.8.

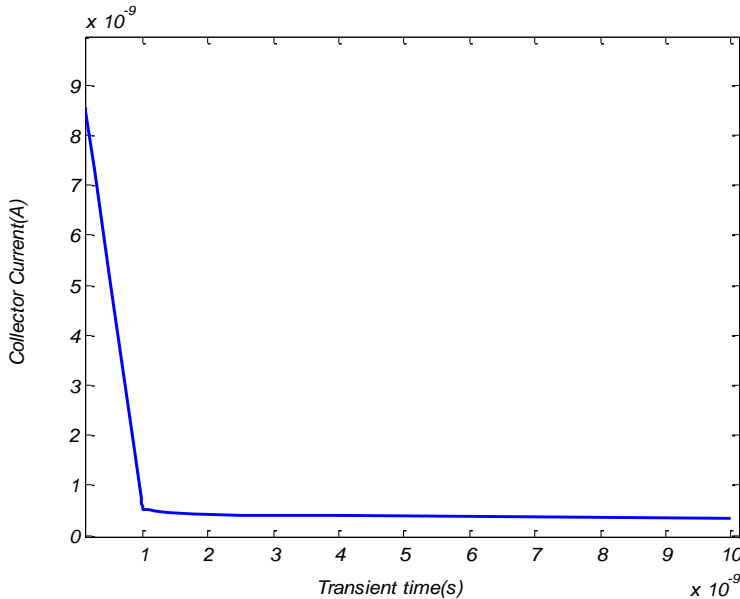


**Figure.8.** Diagram of collector current versus transient time

As seen, the current reaches from a maximum value to a minimum value of  $10^{-10}$  in time of  $10^{-8}$ . The cut off time of this device is 1ns. Figure.9 shows the curves of available photo current, light source photo current and collector current versus transient time. The time axis is in logarithmic scale.

The light is emitted from a distance of 100 nm and in angle of 90 degrees on top of the device. One of the issues seen in figure.9 is that the optical currents follow almost each other and their values reach to value of zero approximately but the collector current still shows a very small value. In fact, figure.9 show the switching characteristics of the device's optical current with light radiation and without light radiation.

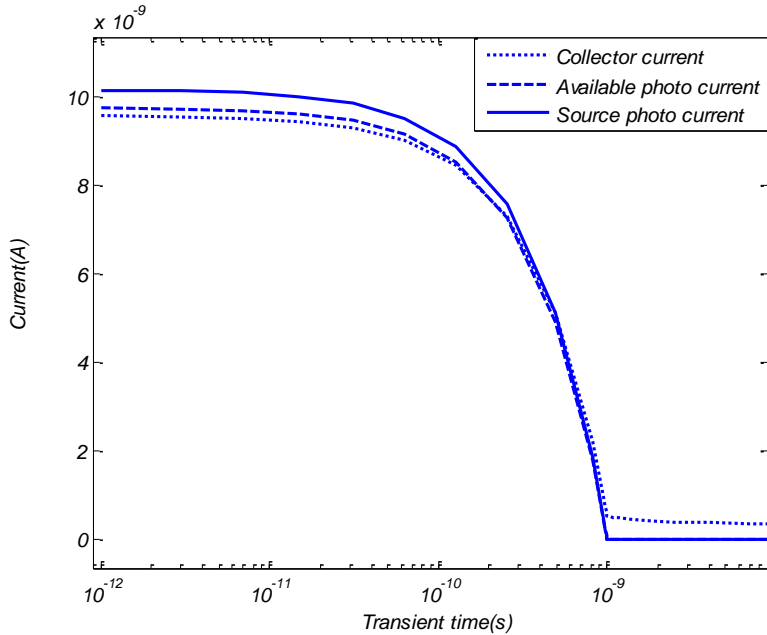


**Figure.9.** Source photo current available photo current and collector current

The energy of light is less than the bandgap energy of the absorption layer and it is not able to produce photo generated carriers due to the effect of light conduction in the absorption layer, because there is an intrinsic current in the absorption layer and it increases due to piezoelectric effect. When light is emitted to the device, the temperature inside the device increases, creating a polarization that reduces the piezoelectric effect. After polarization decreases, the Fermi surface of the absorption layer increases and more light-induced electrons are generated, resulting a noticeable increase in current. Without radiation, the holes in the absorption layer are confined by the polarizing field, causing a dark current.

Figure.10 shows the transient response diagram of the system at different voltages. As can be seen, for a bias of 0 volt, there is a very low intrinsic current in the device that we mentioned earlier, but from a voltage of 0.5 or higher, the maximum collector current is constant and a saturated state is created. When voltage increases, fall time decreases, a steeper slope occurs in the diagram, and the reliability of the device increases and the device response is faster. As seen in figure.9, source photo current, available photo current and collector terminal photo current follow each other, indicating high quantum efficiency of the device.

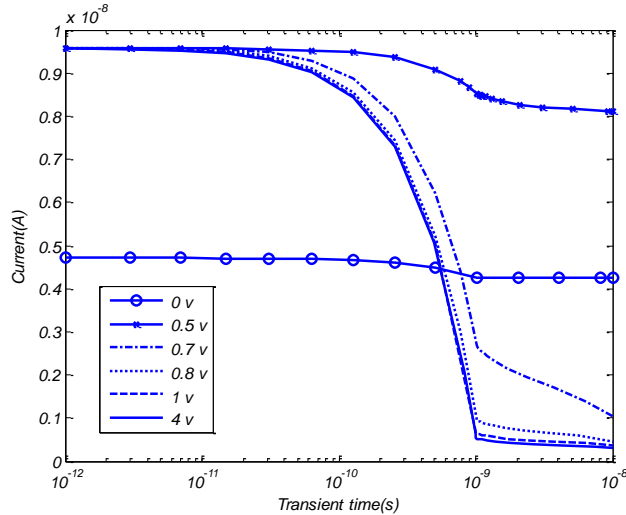


**Figure.10.** Collector current versus transient time versus different voltages

Table.3 shows the collector terminal current values at different times and the times when the current values reach 90% and 10% of the steady state.

**Table 3**

The variations of collector current versus time in different voltage

Voltage(vol t)	90% of steady state(time)	10% of steady state(time)	Time differences
4	$1.2 \times 10^{-10}$	$9 \times 10^{-10}$	$1.27 \times 10^{-10}$
1	$1.2 \times 10^{-10}$	$9.4 \times 10^{-10}$	$7.5 \times 10^{-10}$
0.8	$1.27 \times 10^{-10}$	$1.023 \times 10^{-9}$	$8.96 \times 10^{-10}$
0.7	$1.5 \times 10^{-10}$	$1.3 \times 10^{-8}$	$128.5 \times 10^{-10}$
0.5	$1.02 \times 10^{-9}$	high	high

We changed the physical parameters of the device, and we showed its effects on the transient time response. Figure.11 shows the transient response time diagram of the device at different thicknesses of the adsorption layer. The thicknesses were 100, 200, 400 and 600 nm, respectively. The bias voltage is 2 volts. The fall time decreases as the thickness of the adsorption layer decreases, a steeper slope occurs in the related curve, and the reliability of the device increases. The device response also is faster. It should be noted that better flow is seen in the device with a thickness of 600 nm, but due to the increase in series resistance that causes a decrease in responsivity, the thickness of the absorption layer for this device was not considered more than 600 nm.

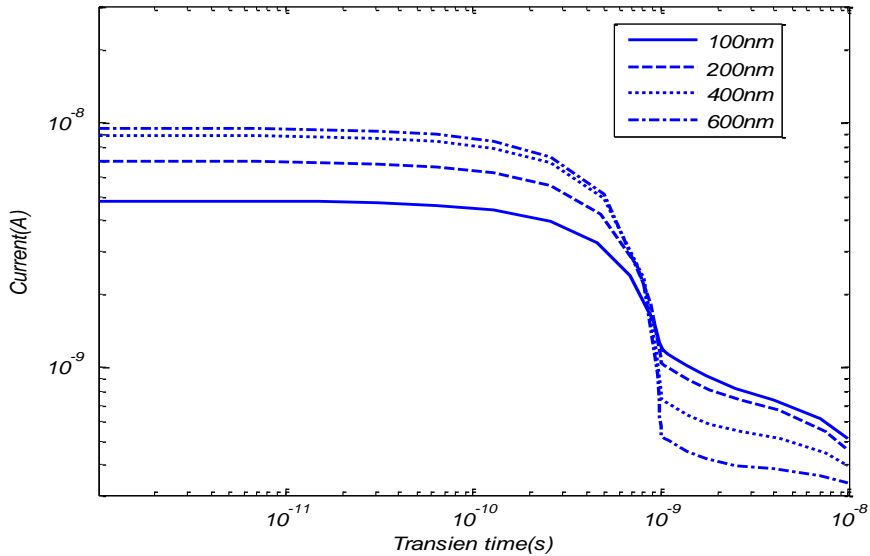


**Figure.11.** Transient response of the device with changes in the thickness of the absorption layer in the bias voltage of 2 volts

The values of the times when the current value reaches 90% and 10% of the steady state have been shown in Table.4

**Table 4**

Time values of 90% and 10% of the steady state of current in different values of the thickness of the adsorption layer

Absorption layer thickness(nm )	90% of steady state(s)	10% of steady state(s)	Time differences(s)
100	$1.4 \times 10^{-10}$	$2 \times 10^{-8}$	$198.6 \times 10^{-10}$
200	$1.27 \times 10^{-10}$	$3.5 \times 10^{-9}$	$33.73 \times 10^{-10}$
400	$1.2 \times 10^{-10}$	$9.3 \times 10^{-10}$	$8.1 \times 10^{-10}$
600	$1.15 \times 10^{-10}$	$9 \times 10^{-10}$	$7.85 \times 10^{-10}$

Figure.12 shows the variations of fall time versus different absorption layer thicknesses. As seen, with increasing of absorption layer thickness, the fall time decreases exponentially. Figure (12) shows that there is an exponential relationship between the fall time and the thickness of the adsorption layer.

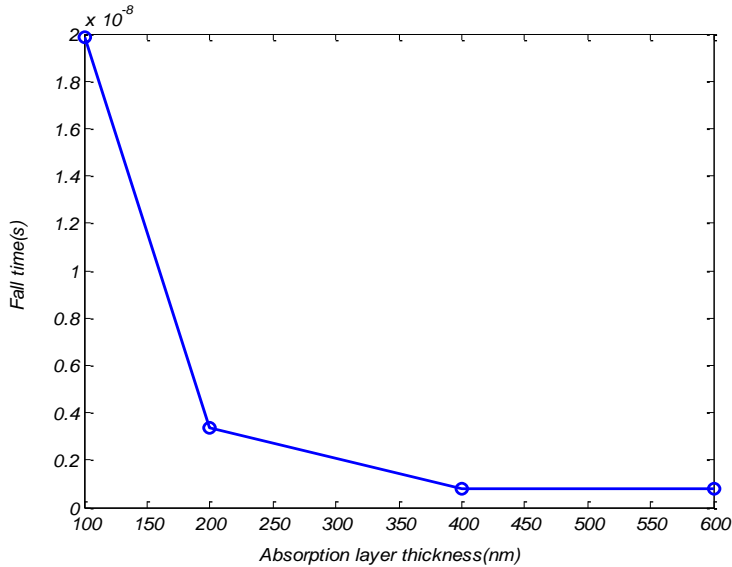


**Figure12.** Fall time according to different thicknesses of the absorption layer at 2V bias voltage

we changed the light intensity and showed its effects on the transient time response of the device. As the light intensity increases, more carriers are created in the absorption area and therefore series resistance in the device decreases and as a result the current increases. A decrease in the resistance of this region indicates an increase in response speed. Figure.13 shows a transient time response at different light intensities emitted from the light source. The bias voltage is 2 volts and the light intensities are 1, 3, 5, 10 Watt per square centimeter. The horizontal and vertical axes are not logarithmic. Table.5 shows the variations of time with different light intensities when the current value reaches 90% and 10% of the steady state quantity.

**Table 5**

Time values of 90% and 10% of the steady state of current in different values of the light intensities

Absorption layer thickness(nm)	90% of steady state(s)	10% of steady state(s)	Time differences(s)
1	$1.2 \times 10^{-10}$	$9.6 \times 10^{-10}$	$8.4 \times 10^{-10}$
3	$1.27 \times 10^{-10}$	$9.5 \times 10^{-10}$	$8.23 \times 10^{-10}$
5	$1.2 \times 10^{-10}$	$9.3 \times 10^{-10}$	$8.1 \times 10^{-10}$
10	$1.25 \times 10^{-10}$	$9 \times 10^{-10}$	$7.85 \times 10^{-10}$

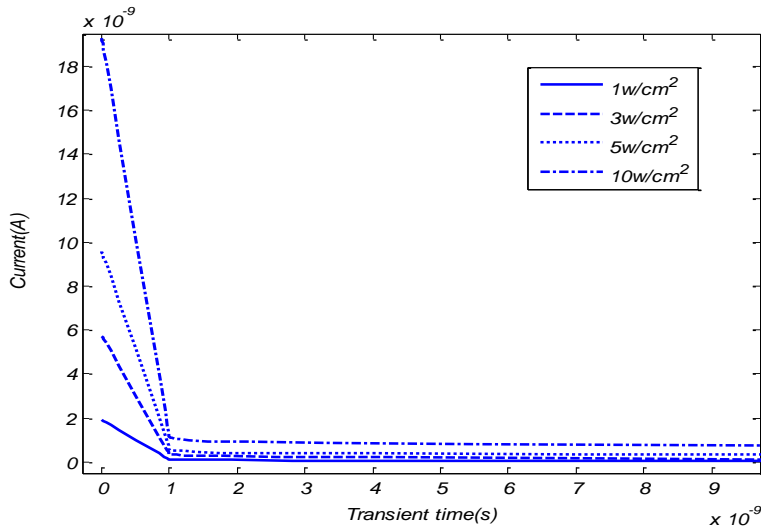


**Figure.13.** Transient time response at different light intensities at 2V bias

The fall times discussed in the previous sections are the device recovery times. The device response time can be obtained in ascending mode response. Figure.14 shows the time response curve in the ascendant response mode of the device.

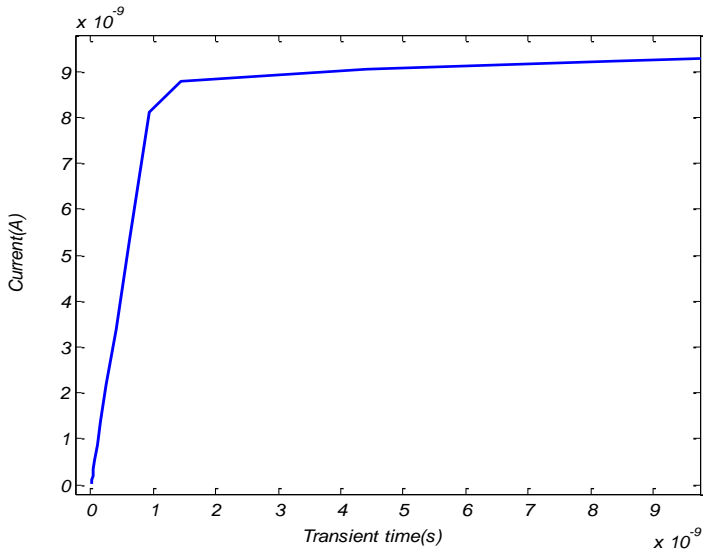


**Figure.14.** Time response of RTD-PD in ascendant mode

Rising time for this device is approximately  $6.2 \times 10^{-10}$  s and, it gives approximately 564 MHz bandwidth.

Changes in the transient time response of the device to changes in the angle of light emitted on the device can be examined. The producing of electron and holes in the absorption layer depends on the angle of radiation. Figure.15 shows this in the form of a diagram.

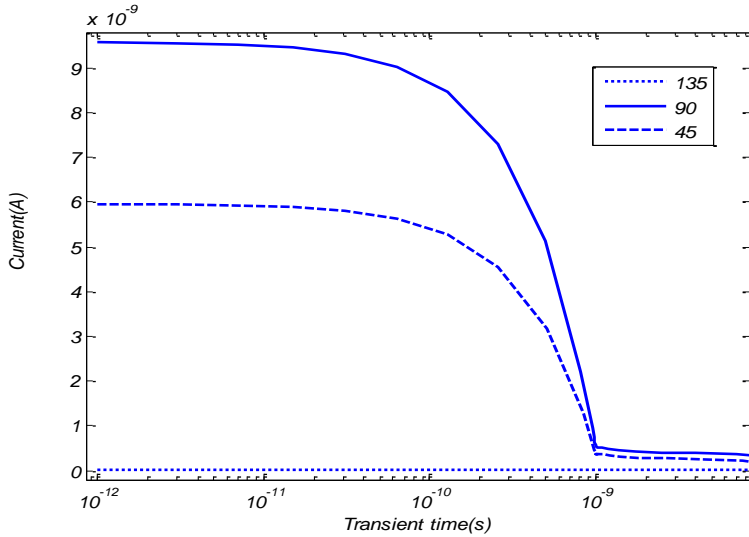


**Figure.15.** Transient time response of the device by changing the angle of light radiation on the device

Figure.15 shows that when light emits at a 90-degree angle on the device, more light-induced electron and hole pairs are created within the absorption layer, which ultimately increase the current in the device. Any deviation from the angle of 90 degree reduces the current, which is confirmed by Figure.14. It is also effective on rise time. Table (4-13) shows the values of rise time and bandwidths obtained by changing of the radiation angle.

**Table 6**

Values of rise time and bandwidth by changing the radiation angle

Angle of radiation( $^{\circ}$ )	Rise time	Bandwidth (MHz)
45	$6.7 \times 10^{-10}$	522
90	$6.2 \times 10^{-10}$	564
135	---	Very low

\*The level of time response is very low

Any deviation from the 90-degree radiation angle will reduce the bandwidth of the device.

Doping of contact layers can also affect the transient time response. Figure.16 shows the transient time response changes with changing the Doping of the contact layers. The ascent cycle is considered in the transient time response which is approximately equal to the descent cycle.

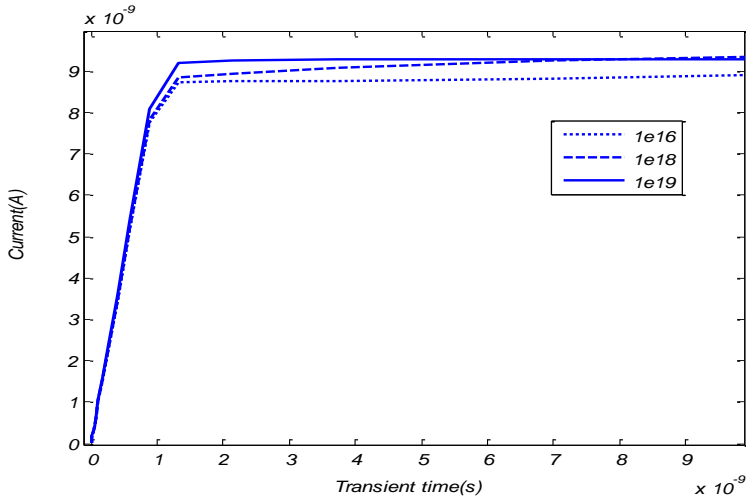


**Figure.16.** Transient time response of the device by changing the doping of the contact layers at the voltage of 2 volts

With the change in doping, the current levels are slightly different, and little effect on bandwidth was observed after  $10^{18}$  concentration. Table .7 shows the rise time bandwidth values of the device.

**Table 7**

Rise time and bandwidth values by changing the concentrations of contact layers

Doping (/cm <sup>3</sup> )	Rise time	Bandwidth (MHz)
$10^{16}$	$6.3 \times 10^{-10}$	555
$10^{18}$	$6.2 \times 10^{-10}$	564
$10^{19}$	$6.2 \times 10^{-10}$	564

As doping concentration decreases, the series resistance of the device increases and bandwidth decreases. After the  $10^{18}$  concentration, there is a very small change in bandwidth. Figure.17 shows the bandwidth changes based on the concentration of the contact layers.

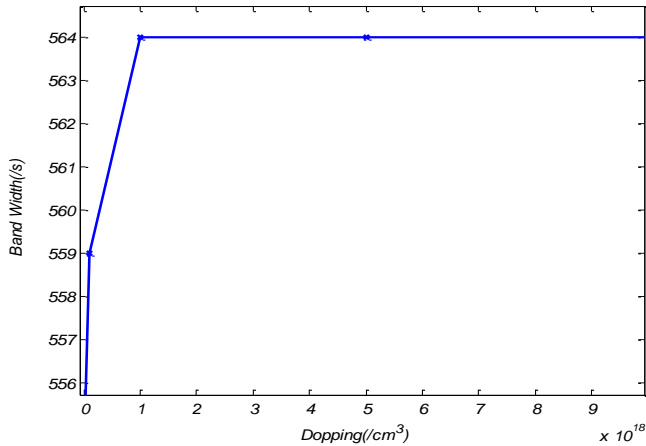


**Figure.17.** Bandwidth variations based on contact layer doping concentrations

#### 4. Conclusion

In this article, the dependencies of the time response of a resonance tunneling diode based photo detector on some parameters were investigated. An effective method was used in this work for designing the device. Energy band diagram and the electric field through the structure was presented. It was found that electric field in the barriers is more than the other layers. As an advantage, significant performance was observed in the proposed device. The quantum efficiency of 0.95 was obtained for the device at room temperature. The curve of transient time response was presented and analyzed. Fall time was calculated. The analysis showed with increasing of voltage bias fall time decreases and the reliability of the device increases and time response of the device is faster. We changed the thickness of absorption layer from 100nm to 600nm. With increasing of absorption layer thickness, a steeper slope occurs and the device response is faster. With increasing of absorption layer thickness, the fall time decreases exponentially. We changed light intensity from 1 to 10  $\text{w/cm}^2$ . Analysis of time response versus variations of light intensity showed that with increasing of light intensity, fall time in transient response decreased. The device response time was obtained in ascending mode response. The angle of emitted light on top of the device can effects on response time. The angles of 45, 90 and 135 degrees were selected. We found that any deviation from the angle of 90 degree reduces the current and it is also effective on rise time and bandwidth. In angle of 90 degrees the bandwidth of 564MHz was obtained. Doping concentration of contacts layers were changed. The result showed that with decreasing of doping concentration of contact layer, there were small changes in bandwidth and current levels.

**References:**

- [1] Granastein, V. L. *Physical Principles of Wireless Communications*; CRC Press: Boca Raton, FL, USA, 2012; pp. 171–201.
- [2] M. Sauer, A. Kobayakov, J. George. *Radio over fiber for Pico cellular network architectures. J. Lightware Technol.* 25, 2007, 3301–3320.
- [3] N.J. Gomes, M.Morant, A. Alphones, B.Cabon, J.E.Mitchell, C.Lethien, M. Csornyei, A.Stohr, S.Iezekiel. *Radio-over-fiber transport for the support of wireless broadband services. J. Opt. Netw.* 8, 2009,156–178.
- [4] S. Salimi, H.Rasooli Saghai. *Impressive Reduction of Dark Current in InSb Infrared Photodetector to achieve High Temperature Performance.* Journal of optoelectronic nanostructures, Vol.3, No.4, (2018), 81-96.
- [5] M. Klemm, M.; J.A. Leendertz, D.Gibbons, I.J.Craddock, A.Preece, R.Benjamin. *Microwave radar-based breast cancer detection: Imaging in inhomogeneous breast phantoms.* IEEE Ant. Wirel. Propag.Lett. 8, 2009, 1349–1352.
- [6] Haidong Lu, Bin Zhang, Fangmin Guo. *The Photocurrent-Voltage characteristic simulated of resonant tunneling photodiodes.* Optical and Quantum Electronics (2016). Available: <http://doi.org/10.1007/s11082-016-0373-9>
- [7] Scott Watson, Weikang Zhang, Joana tavaréz, Jose Figueiredo, H. Canta, Jue Wang, Edward wasige, Henrique Salgado, Luis Pessoa and Antohony Kelly. *Resonant tunneling photodetectors for optical communications.* Microwave and Optical Technology Letters (2019). Available: <https://doi.org/10.1002/mop.31689>.
- [8] Micheal Feginov. *Frequency Limitations of Resonant-Tunneling Diodes in Sub-THz and THz Oscillators and Detectors.* Journal of infrared, millimeter, and terahertz waves, vol.40, (2019), 365-394.
- [9] Bruno Romeria, LM Pessoa, H.M. Salgad, C.N. Ironside and Jose M.L Figueiredo. *photo detectors Integrated with resonant tunneling diode.* Sensors, vol.13, (2013), 9464-9482.
- [10] Rania Mohammad Abdallah, Ahmed Ahmed S. Dessouki M. Hussein Aly. *The Resonant Tunneling Diode Characterization for high frequency Communication Systems.* Microelectronic Journal, vol.75, (2018), 1-14.
- [11] Saad G Muttlac, Omar S. Abdulwahid, J Sextor, Michael J. Kelly and Mohamed Missous. *InGaAs/AlAs Resonant Tunneling diodes for THZ Application.* IEE Journal of the Electron Devices Society, Vol.6, (2018), 254-262.
- [12] Xiang yang shi, Yuan yuan Wu, Ding Wang, Juan Su, Jie Liu, Wen Xian Yang, Meng Xiao and Jian Zhang. *Enhancing power density of strained In<sub>0.8</sub>Ga<sub>0.2</sub>As/AlAs RTD for tera hertz radiation by optimizing emitter*

- spacer layer thickness*. Supper lattices and Micro Structures, vol.12, (2017), 435-441.
- [13] Man Mohan singh and M.J. siddigui. *Electrical characterization of triple barrier GaAs/AlGaAs RTD with dependence of operating temperature and barrier lengths*. Material science in semiconductor processing, vol.58, (2017), 89-95.
- [14] Shofa Abdullah Almansour and Dakhlaoui Hassan. *Resonant tunneling diode Photodetector operating at near infrared wavelength with high responsivity*. Optics and Photonics Journal, vol.4, (2014), 39-45.
- [15] Andreas pfenning, F. Hartman, F. langer, Martin kanp, Sven Hofling and f. Lukas worschech. *Sensevity of resonant tunneling diode photodectors*. Nano technology, vol. 27, No. 35, (2016), 1-9.
- [16] Y Dong, Guanglong Wang, Haiqiao Ni, Jianhui Chen, Fengqi Gao, Baochen Li, Kangming Pei and Zhichuan Niu. *Resonance Tunneling Diode Photodetector with non-constant responsivity*. Optic communications, vol.335, (2015), 274-278.
- [17] Andreas Pfenning, Fabian Hartmann, Mariama Rebello Sousa Dias, Fabian Langer, Martin Kamp, Leonardo Kleber Castelano, Victor Lopez-Richard, Gilmar Eugenio Marques, Sven Höfling, and Lukas Worschech. *Photocurrent-voltage relation of resonant tunneling diode photodetectors*. Applied Physics Letters.107, (2015), 081104.
- [18] Yu Dong, Jianxing Xu, Guanglong Wang, Haiqiao Ni, Kangming Pei, Jianhui Chen, Fengqi Gao, Baochen Li and Zhichuan Niu. *Resonant tunneling diode Photodetector operating at near infrared wavelength with high responsivity*. Electronic Letters, Vol.51, No.17, (2015), 1355-1357.
- [19] Andreas pfenning, F. Hartman, F. langer, Sven Hofling and Martin Kamp.: *Cavity enhanced RTD-PD telecommunication wavelength*. Applied Physics.letters.104, (2014), 101109.
- [20] Yo Dong, Gauglong wang, Hiqiao Ni, Jianhui Chen, Fengqi Gau, Zhongtao Qiao and Zhichuan Niu. *Resonant tunneling diode with a multiplication region for light detection*. Optics communications, Vol.331, (2014), 94-97.
- [21] F. Hartmann, F.Langer, D.Bisping, .Musterer, S.Höfling, M.Kamp, A.Forchel and Worschech. *GaAs/AlGaAs resonant tunneling diodes with a GaInNAs absorption layer for telecommunication light sensing* Appl.Phys, Lett.100, (2012), 172113.
- [22] H.W. Li, B.E. Kardyna, P. See, A.J. Shields, P. Simmonds, H.E. Beere and D.A. Ritchie. *Quantum dot RTD for telecommunication wavelength single photon detector*. Appl. Phys. Lett. 91, (2007), 073516.
- [23] W. Zhang, Scott Watson, Jose Figueiredo, Jue Wang, H. Cantu, J.Tavarez, L.Pessoa, A.Khalid, H.Salgado, E.Wasige and A.E.Kelly. *Optical direct*

- intensity modulation of a 79GHz resonant tunneling diode-photodetector oscillator*. Optics Express, Vol.27, No.12, (2019), 16791-16797.
- [24] Junzhe zheng et al. *Quantitative Multi-Scale, Multi-Physics Quantum Transport Modeling of GaN-Based Light Emitting Diodes*. Physica status solidi, Vol.215, No.9, (2017).
- [25] K.C. Wang, R.Grassi,Y.Chu, S.Hari, J.Geng. *Introduction of Multi-Particle Probes – Bridging between Drift Diffusion and Quantum Transport*. arXiv:2001.04391v1, physics.app-ph, (2020).
- [26] U. Aeberhard. *Challenges in the NEGF Simulation of Quantum-Well Photovoltaics Posed by Non-Locality and Localization*. Physica status solidi, Vol.256, No.7, (2019).
- [27] T. martin, P.Dixon. *InGaAs sees infrared and visible light*. Laser focus, Vol.40, No.11, (2004), 109-111.
- [28] J. Zou, D.J.H. Cockyan and B.F. Usher. *Misfit dislocation and critical thickness in InGaAs/GaAs heterostructure systems*. Journal of Applied Physics, Vol.73, No.619, (1993).
- [29] Mohammad Hasani, Raad Chegell. *Electronic and Optical Properties of the Graphene and Boron Nitride Nanoribbons in Presence of the Electric Field*. Journal of optoelectrical nanostructures, Vol.5, Issue.2, (2020), 49-64.
- [30] Hamid Faezinia, Mahdi zavvari. *Quantum modeling of light absorption in graphene based photo- transistor*. Journal of optoelectrical nanostructures, Vol.2, No.1, (2017), 9-20.
- [31] Atlas, [www.silvaco.com](http://www.silvaco.com), (2016).
- [32] M.M. Singh, M.J. Siddiqui, A.Saxena. *Effect of Si-delta doping of barrier lengths on performance of triple barrier GaAs/AlGaAs RTD*. IEEE international conference on electron devices and Solid-state circuits, (2016), 581-587.